Electronic Supplementary Material (ESI) for Organic & Biomolecular Chemistry.

Mononuclear Iron(III) Complexes of Tridentate Ligands with Efficient Nuclease Activity and Studies on their Cytotoxicity

Nidhi Tyagi,[a] Ajanta Chakraborty[b], Udai P. Singh,[a] Partha Roy*,[b] Kaushik Ghosh,*[a]

[a]Department of Chemistry, Indian Institute of Technology Roorkee, Roorkee-247667

Uttarakhand INDIA. E-mail: ghoshfcy@iitr.ernet.in

[b]Department of Biochemistry, Indian Institute of Technology Roorkee, Roorkee-247667

Uttarakhand INDIA. E-mail: paroyfbt@iitr.ernet.in

a)

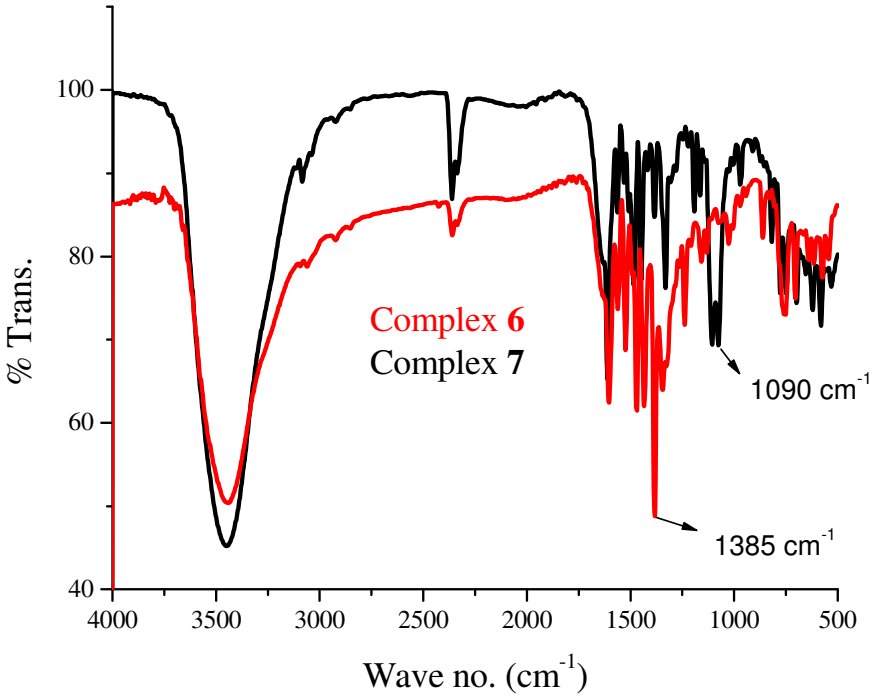
100
80
60
40
% Trans.
4000
3500
3000
2500
2000
1500
1000
500
Wave no. (cm-1)
Complex 6
Complex 7
1090 cm-1
1385 cm-1

b)

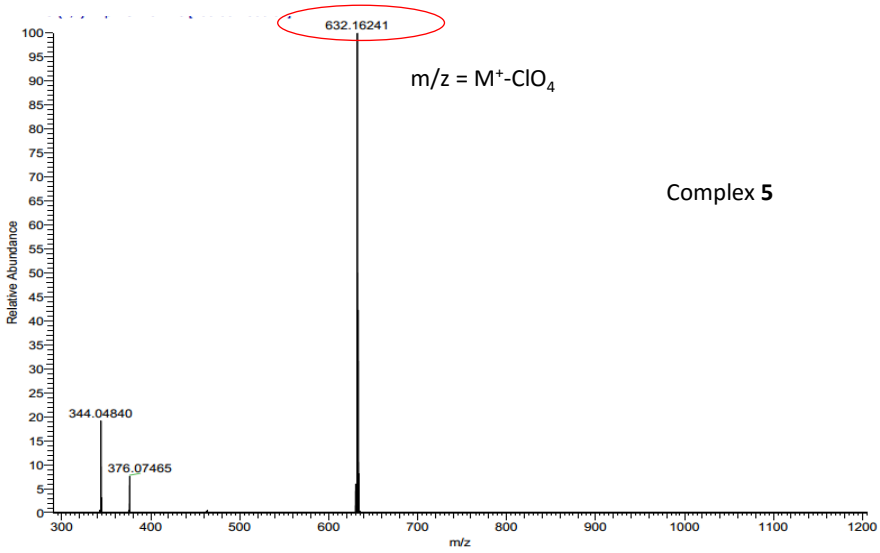
632.16241
m/z = M+-ClO4
Complex 5
Relative Abundance
344.04840
376.07465
m/z

c)

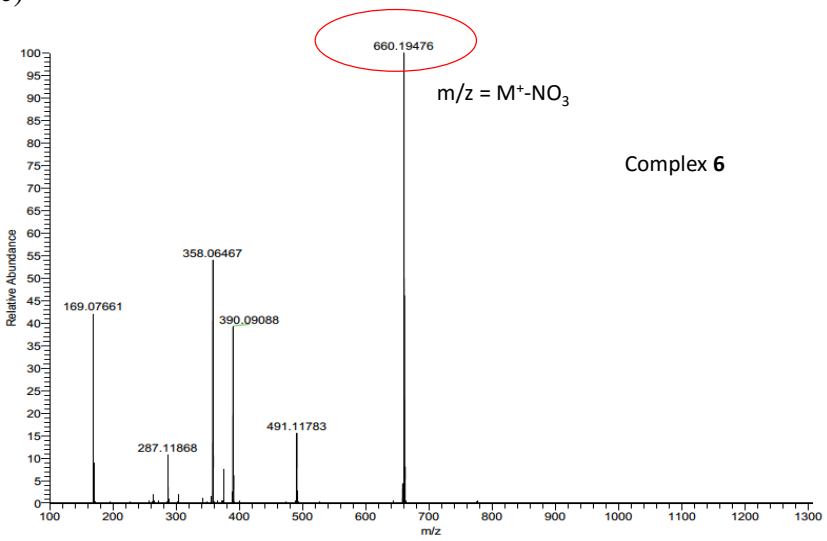
660.19476
m/z = M+-NO3
Complex 6
358.06467
169.07661
390.09088
491.11783
287.11868
Relative Abundance
m/z

d)

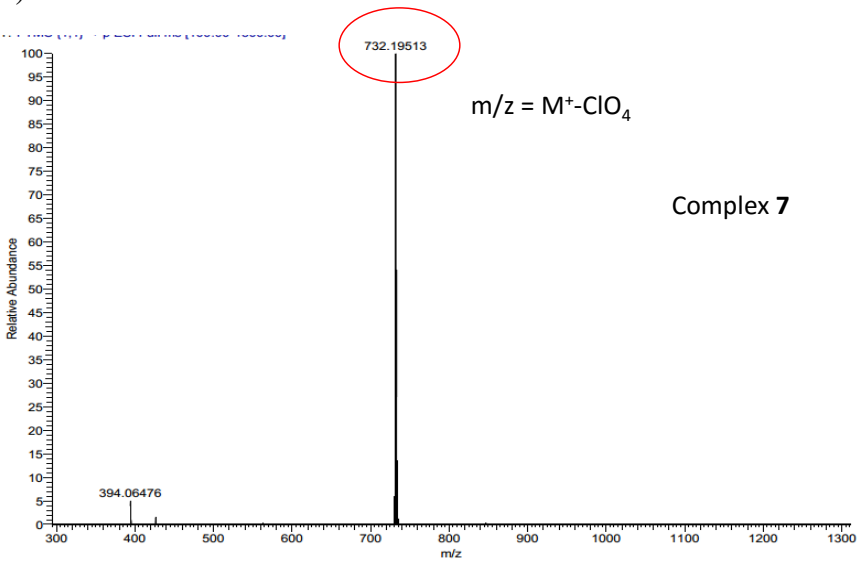
732.19513
m/z = M+-ClO4
Complex 7
394.06476
Relative Abundance
m/z

e)

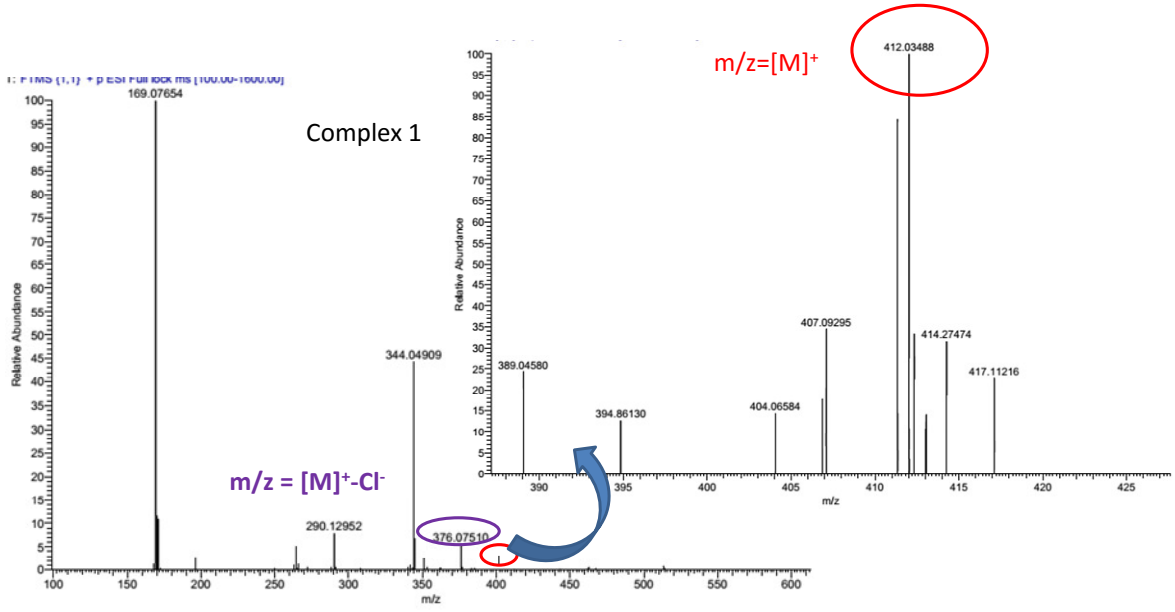
169.07654
Complex 1
m/z=[M]+
412.03488
344.04909
m/z = [M]+-Cl-
290.12952
376.07510
389.04580
394.86130
404.06584
407.09295
414.27474
417.11216
Relative Abundance
m/z

f)

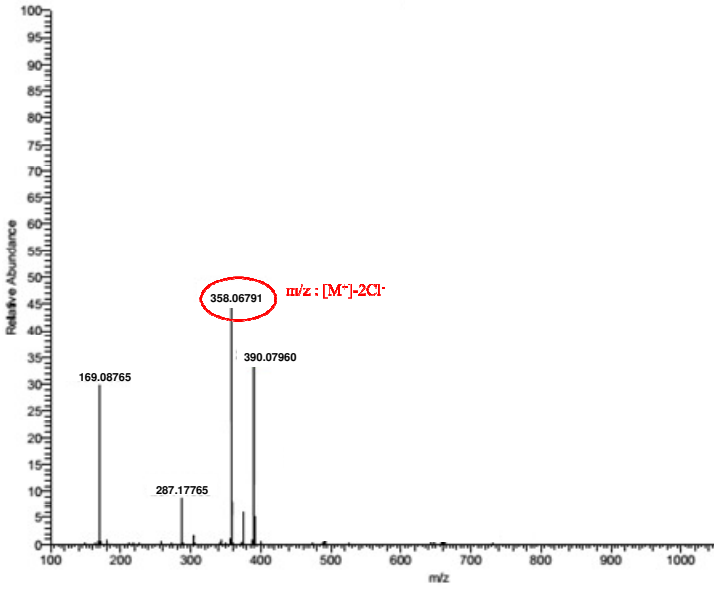

Fig. S1 a) IR spectra of representative complexes (**5** and **6**) b-f) ESI-MS spectra of complexes **5**, **6**, **7**, **1** and **3.**

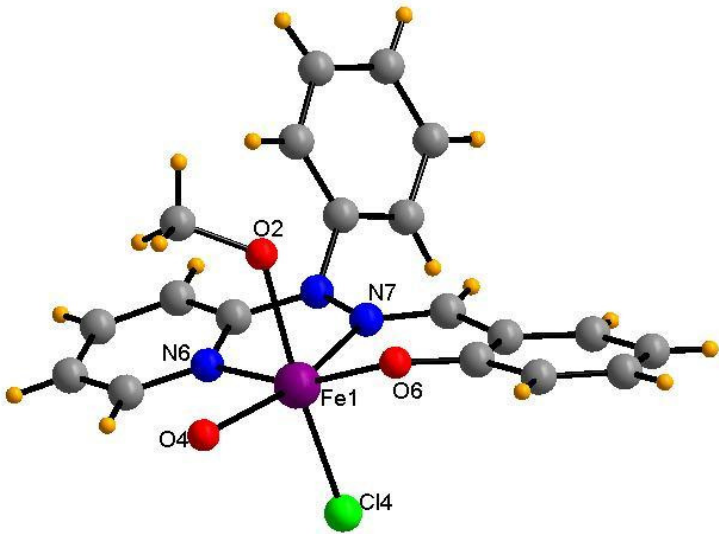

Fig. S2 Ball-and-stick representation of the crystal structure of complex [Fe(Phimp)(OMe)(H_2O)Cl], **1** atoms are shown as sphere of arbitrary diameter

Crystals of complex **1** were obtained from a solvent mixture of methanol:dichloromethane (1:1) by diethylether diffusion at -10 ^{o}C. Selected bond lengths, bond angles and crystallographic data for **1** is given in Table S3-S4. In **1**, iron centre exhibits a distorted octahedral geometry comprising tridentate ligands ($Phimp^{-}$), a water molecule (H_2O) at equatorial position, deprotonated methanol (-OMe) and chloride (-Cl) in axial position. Complex **1** showed two molecules in a unit cell in which one molecule has thermal error in one phenyl ring. The apical site was occupied by a chloride ion. The Fe–O_{ph} distances in **1** is 1.915(4) Å. Fe-N_{im} and Fe-N_{py} distances were approximately equal (Fe1-N7: 2.154(5) Å, Fe1-N6: 2.128(6) Å.

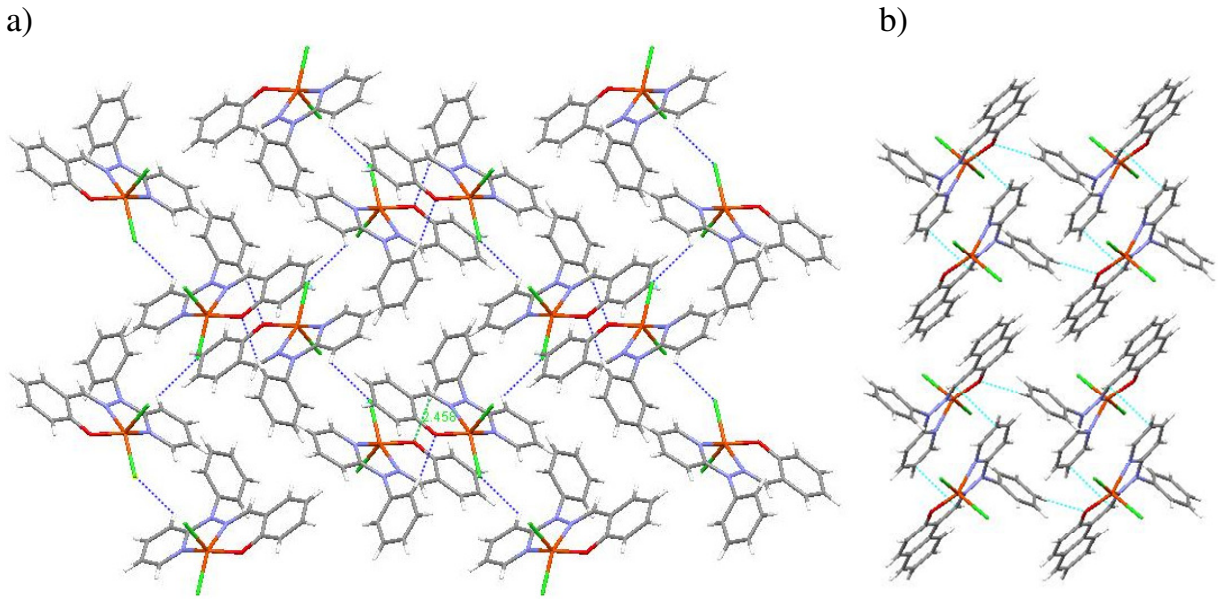

Fig. S3 Packing diagram of complexes **2** and **4** showed the non-covalent interaction between a) Cl-H_{py} and O-H_{Ph} (for **2**), b) O-H_{Ph} and C_{aryl}-C_{imine} (for **4**), along *a* axis.

a)

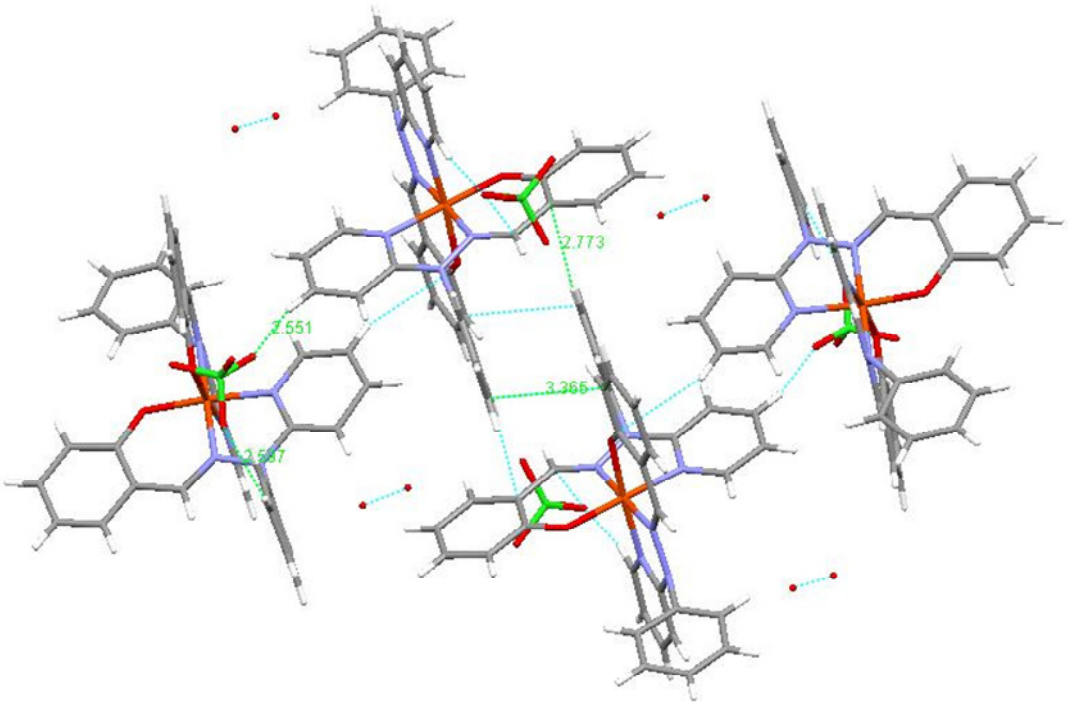

b)

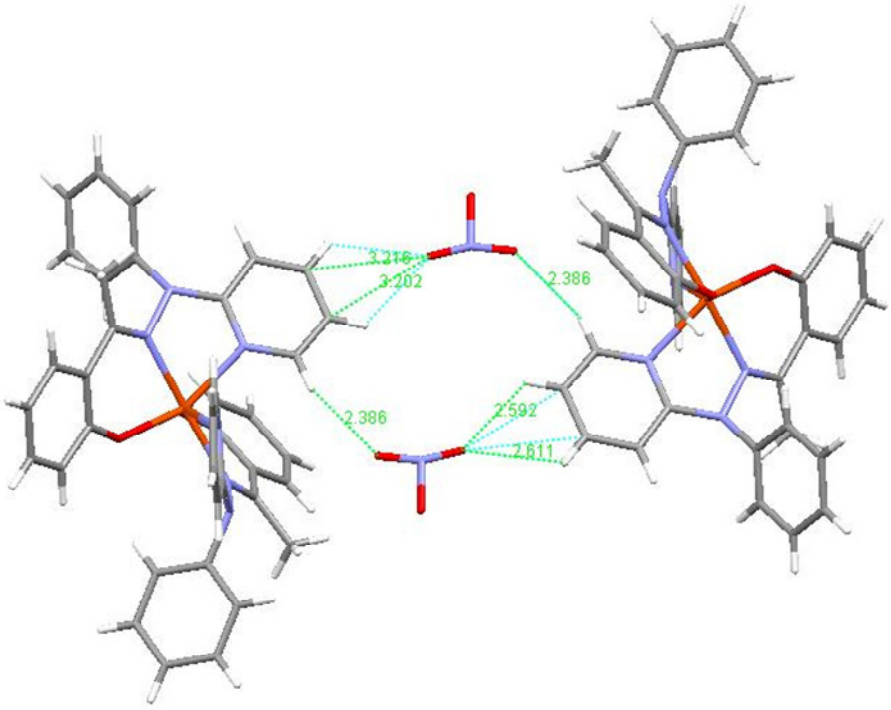

Fig. S4 Diagram showing non-covalent interaction in the complexes **5** and **6**

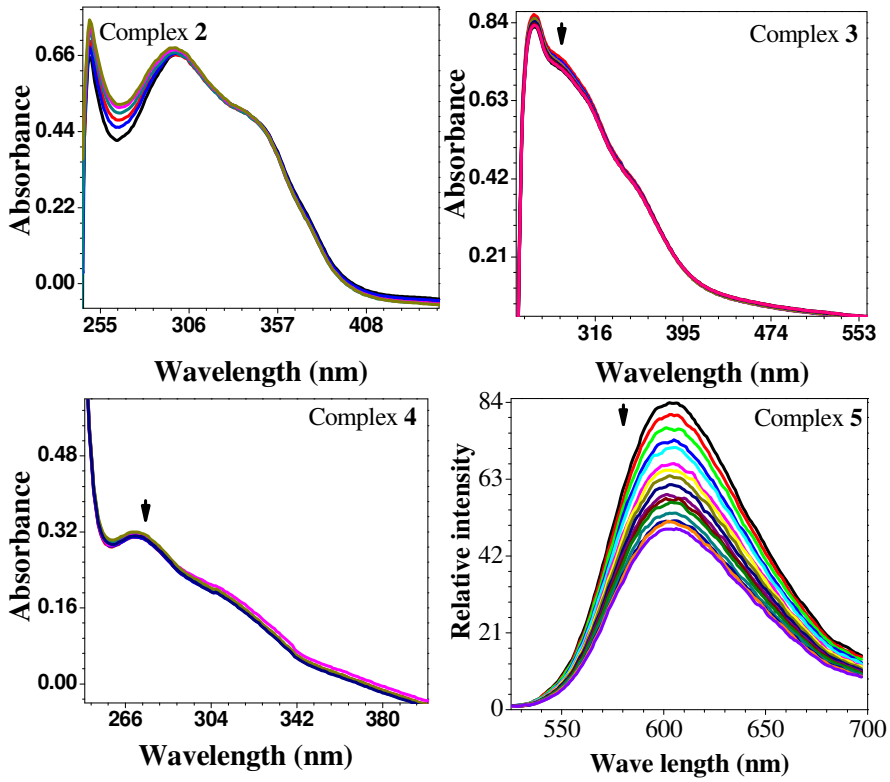

Fig. S5 a, **b**) Absorption spectra in 0.1 mM phosphate buffer (pH 7.2) in presence of increasing amounts of DNA ([DNA] ~ 0-100 μM) for complex **2**-**4**; **c**) EtBr–DNA fluorescence quenching titrations of complex **5** (0-50 μM), Tests was performed in the conditions of 50 mM phosphate buffer (pH 7.2) at 298 K. C_{DNA} = 25 μM, C_{EtBr} = 0.5 μM; λ_{ex} = 250 nm, λ_{em} = 602 nm.

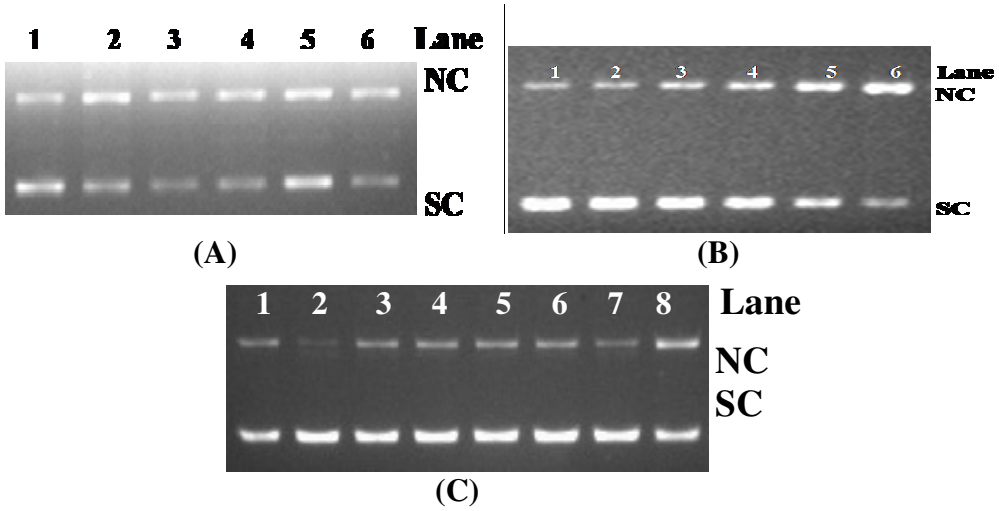

Fig. S6 Gel electrophoresis separations showing cleavage of supercoiled *pBR322* DNA (60 ng) by complexes **4**, **5** and **7** incubated at 37 °C for 3 h. **(A)** lane 1: DNA, lane 2: DNA + BME (200 μM), lane 3: DNA + **4** (200 μM) + BME (200 μM), lane 4: DNA + H_2O_2 (200 μM), lane 5: DNA + **4** (150 μM) + H_2O_2 (200 μM), lane 6: DNA + **4** (200 μM) + BME (200 μM). **(B)** lane 1: DNA, lane 2: DNA + **5** (150 μM), lane 3: DNA + **5** (150 μM) + BME (150 μM), lane 4: DNA + **5** (150 μM) + H_2O_2 (150 μM), lane 5: DNA + BME (150 μM), lane 6: DNA + H_2O_2 (150 μM). **(C)** lane 1: DNA, lane 2: DNA + **7** (100 μM), lane 3: DNA + **7** (100 μM) + BME (100 μM), lane 4: DNA + **7** (100 μM) + BME (150 μM), lane 5: DNA + **7** (100 μM)+ H_2O_2 (100 μM), lane 6: DNA + **7** (100 μM) + H_2O_2 (150 μM), lane 7: DNA + BME (150 μM), lane 8: DNA + H_2O_2 (150 μM).

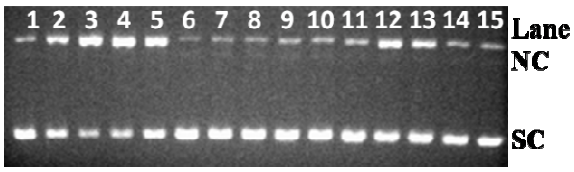

Fig. S7 Gel electrophoresis separations showing cleavage of supercoiled *pBR322* DNA (60 ng) by complexes **2**, **5** and **6** in 10% dimethylformamide incubated at 37 °C for 3 h. lane 1: DNA, lane 2: DNA + **6** (25 μM), lane 3: DNA + **6** (50 μM), lane 4: DNA + **6** (75 μM), lane 5: DNA + **6** (100 μM), lane 6: DNA + **5** (25 μM), lane 7: DNA + **5** (50 μM), lane 8: DNA + **5** (75 μM), lane 9: DNA + **5** (100 μM), lane 10: DNA + **2** (25 μM), lane 11: DNA + **2** (50 μM), lane 12: DNA + **2** (75 μM), lane 13: DNA + **2** (100 μM), lane 14: DNA + Fe(III) salt (100 μM), lane 15: DNA + 10% DMF.

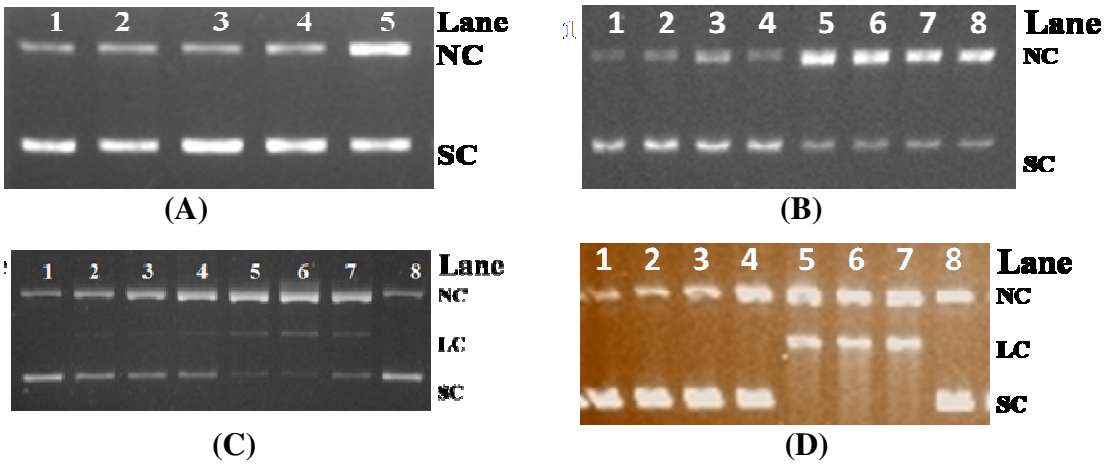

Fig. S8 Gel electrophoresis separations showing cleavage of supercoiled *pBR322* DNA (60 ng) by complexes **1**, **2**, **3** and **6** in 10% dimethylformamide incubated at 37 °C for 3 h. **(A)** lane 1: DNA, lane 2: DNA + H_2O_2 (200 μM), lane 3: DNA + **1** (15 μM) + H_2O_2 (200 μM), lane 4: DNA + **1** (25 μM) **+** H_2O_2 (200 μM), lane 5: DNA + **1** (50 μM) + H_2O_2 (200 μM). **(B)** lane 1: DNA, lane 2: DNA + H_2O_2 (300 μM), lane 3: DNA + **2** (100 μM), lane 4: DNA + **2** (15 μM) + H_2O_2 (300 μM), lane 5: DNA + **2** (25 μM) + H_2O_2 (300 μM), lane 6: DNA + **2** (50 μM) + H_2O_2 (300 μM), lane 7: DNA + **2** (80 μM) + H_2O_2 (300 μM), lane 8: DNA + **2** (100 μM) + H_2O_2 (300 μM). (**C**) lane 1: DNA, lane 2: DNA + **3** (25 μM) + H_2O_2 (150 μM), lane 3: DNA + **3** (50 μM) **+** H_2O_2 (150 μM), lane 4: DNA + **3** (75 μM) + H_2O_2 (150 μM), lane 5: DNA + **3** (100 μM) + H_2O_2 (150 μM), lane 6: DNA + **3** (150 μM) + H_2O_2 (150 μM), lane 7: DNA + **3** (200 μM) + H_2O_2 (150 μM), lane 8: DNA + H_2O_2 (150 μM). **(D)** lane 1: DNA, lane 2: DNA + **6** (10 μM) + H_2O_2 (200 μM), lane 3: DNA + **6** (15 μM) + H_2O_2 (200 μM), lane 4: DNA + **6** (25 μM) + H_2O_2 (200 μM), lane 5: DNA + **6** (100 μM) + H_2O_2 (200 μM), lane 6: DNA + **6** (50 μM) + H_2O_2 (50 μM), lane 7: DNA + **6** (50 μM) + H_2O_2 (200 μM), lane 8: DNA + H_2O_2 (200 μM).

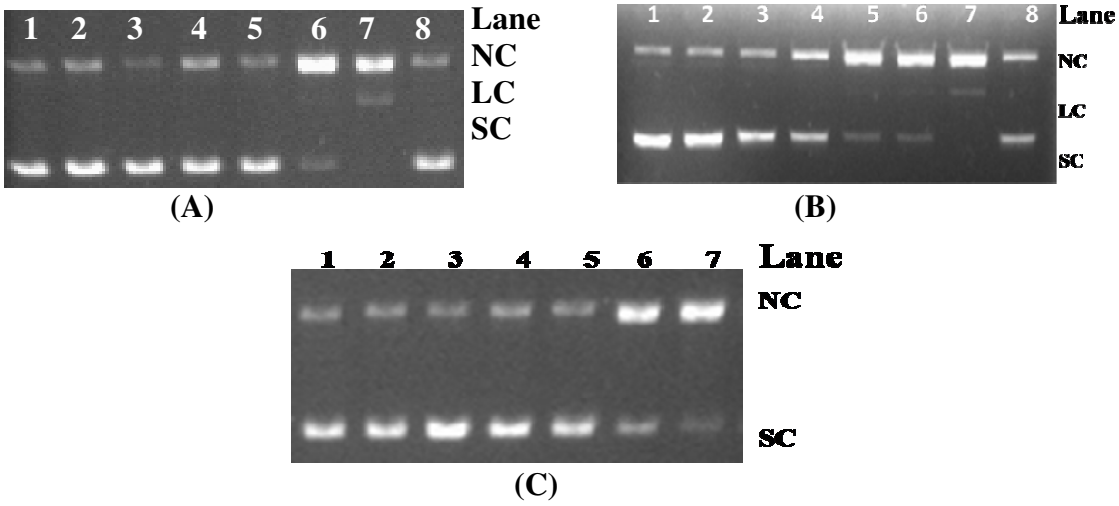

Fig. S9 Gel electrophoresis separations showing cleavage of supercoiled *pBR322* DNA (60 ng) by complexes **1**, **2**, **3** and **6** in 10% dimethylformamide incubated at 37 °C for 3 h. **(A)** lane 1: DNA, lane 2: DNA + **1** + BME (25 μM), lane 3: DNA + **1** (25 μM) + BME (50 μM), lane 4: DNA + **1** (25 μM) **+** BME (100 μM), lane 5: DNA + **1** (25 μM) + BME (200 μM), lane 6: DNA + **1** (50 μM) + BME (200 μM), lane 7: DNA + **1** (75 μM) + BME (200 μM), lane 8: DNA + BME (200 μM). **(B)** lane 1: DNA, lane 2: DNA + **2** (10 μM) + BME (200 μM), lane 3: DNA + **2** (15 μM) + BME (200 μM), lane 4: DNA + **2** (25 μM) + BME (200 μM), lane 5: DNA + **2** (30 μM) + BME (200 μM), lane 6: DNA + **2** (50 μM) + BME (50 μM), lane 7: DNA + **2** (50 μM) + BME (200 μM), lane 8: DNA + BME (200 μM). **(C)** lane 1: DNA, lane 2: DNA + BME (200 μM), lane 3: DNA + **3** (25 μM) + BME (25 μM), lane 4: DNA + **3** (25 μM) **+** BME (100 μM), lane 5: DNA + **3** (25 μM) + BME (200 μM), lane 6: DNA + **3** (50 μM) + BME (200 μM), lane 7: DNA + **3** (75 μM) + BME (200 μM).

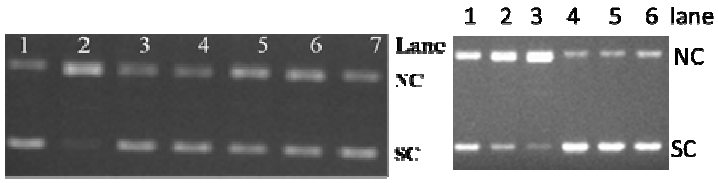

(A) (B)

Fig. S10 Gel electrophoresis separations showing cleavage of supercoiled *pBR322* DNA (60 ng) by complexes **3** and **2** in 10% dimethylformamide incubated at 37 °C for 3 h. A) lane 1: DNA, lane 2: DNA + **3** (50 μM) + BME (200 μM), lane 3: DNA + **3** (50 μM) + BME (200 μM) + KI (20 mM), lane 4: DNA + **3** (50 μM) + BME (200 μM) + DMSO (20 mM), lane 5: DNA + **3** (50 μM) + BME (200 μM) + **NaN_3** (50 mM), lane 6: DNA + **3** (50 μM) + BME (200 μM) + **L-his** (20 mM), lane 7: DNA + **3** (50 μM) + BME (200 μM) + D_2O (20 mM). B) lane 1: DNA, lane 2: DNA + **2** (75 μM), lane 3: DNA + **2** (75 μM) + NaN_3 (50 mM), lane 4: DNA + **2** (75 μM) + + DMSO (20 mM), lane 5: DNA + **2** (75 μM) + D_2O (20 mM), lane 7: DNA + **2** (75 μM) + KI (20 mM).

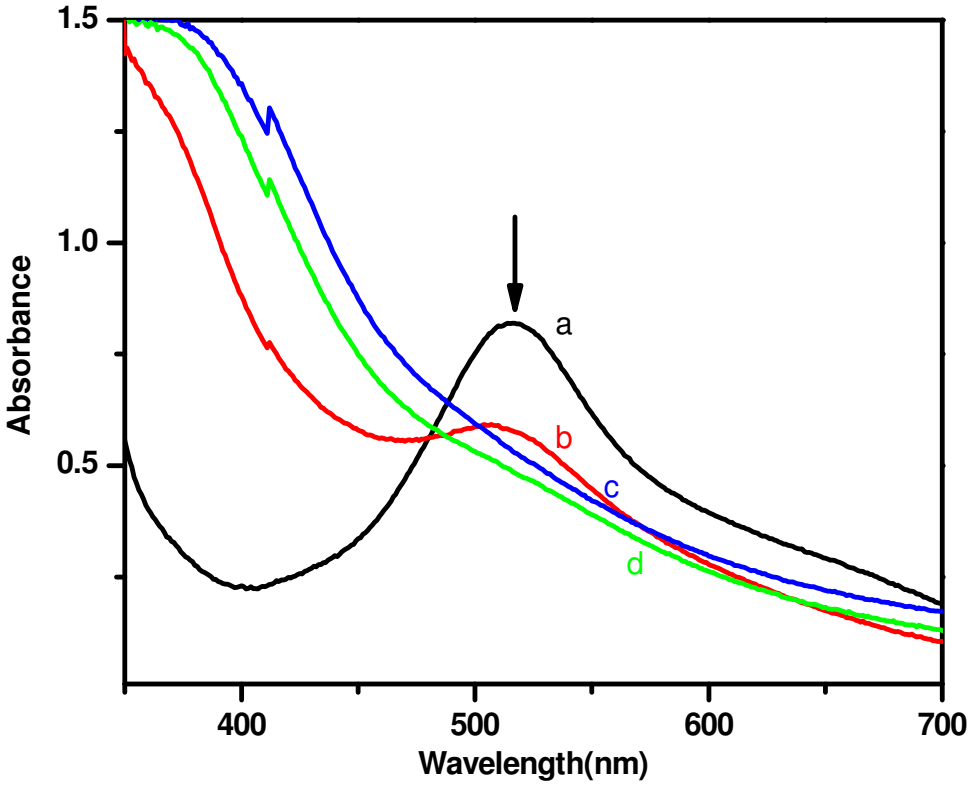

Fig. S11 UV-vis spectra of DPPH (*a*, 60 μM) quenching at 520 nm with increasing concentration of **5** and H_2O_2 (*b*-*d*, 0-150 μM).

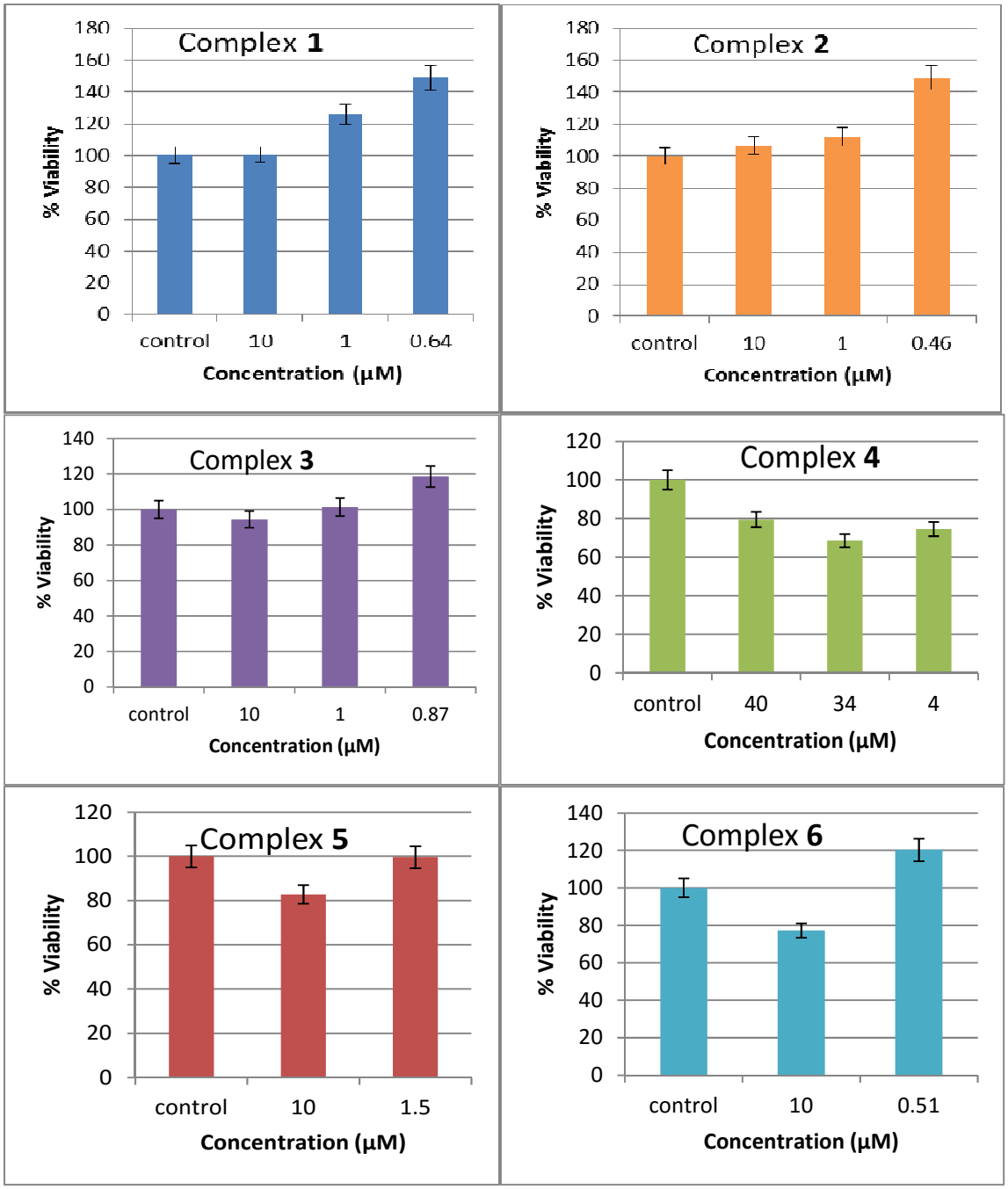

Fig. S12 % viability of complexes (**1-6**) in HEK cell lines.

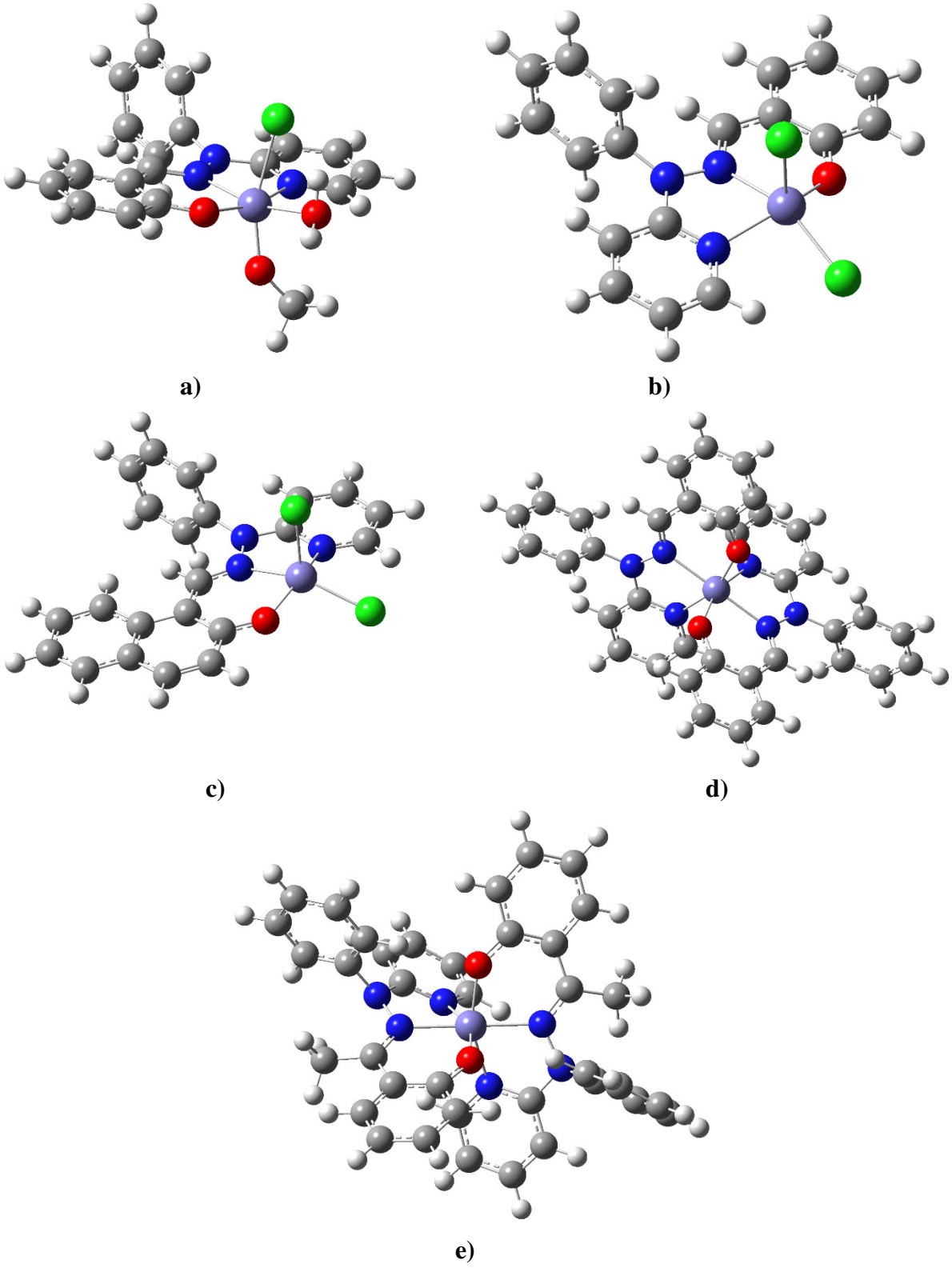

Fig. S13 Optimized structures of complexes **1**-**6.**

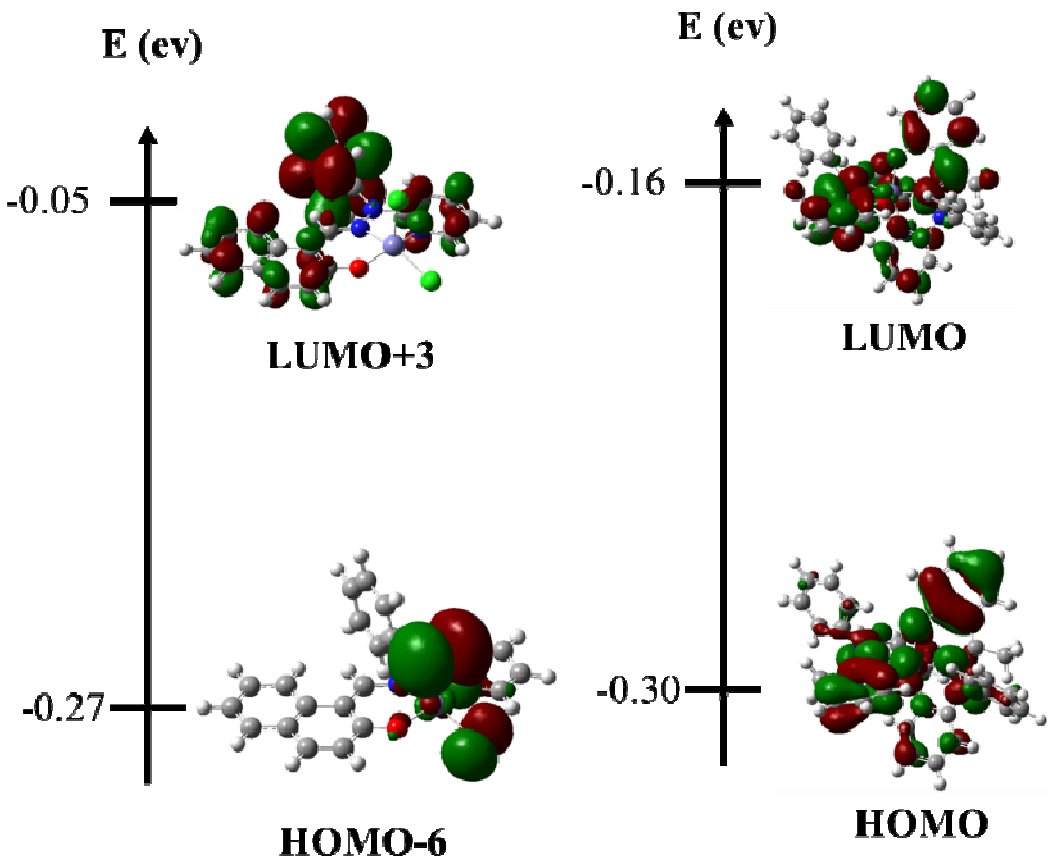

Fig. S14 Diagram showing the relative energies of the highest occupied and lowest unoccupied MOs of complex **4** and **6** transitions responsible for the LMCT absorption in the absorption spectra.

Table S1 Data for IR and conductivity

Complex	IR data (cm^{-1})[a]			Conductivity data ($\Lambda_M/\Omega^{-1}cm^2mol^{-1}$)[b]
	$\nu_{C=N}$	ν_{ClO4^-} /ν_{NO3^-}	ν_{C-C} or $\nu_{C-Naromatic}$	
1	1637	-	1524-1439	17 (neutral)
2	1637	-	1526-1440	18 (neutral)
3	1615	-	1530-1441	30 (neutral)
4	1609	-	1563-1436	18 (neutral)
5	1605	1090, 622	1563-1445	63 (1:1)
6·H_2O	1601	1383	1558-1434	75 (1:1)
7	1608	1089, 622	1563-1446	65 (1:1)

[a] Using KBr pellets, [b]Solvent: dimethylformamide

Table S2. Electrochemical data for Fe(III)/Fe(II) redox couple at 298 K[a] vs Ag/AgCl

S. No.	Fe(III)/Fe(II)			[d]$n=i_{Pa}/i_{Pc}$
	E_{pa}/V	E_{pc}/V	$E_{1/2}$[b], V, (ΔE_p[c], mV)	
Complexe 2	0.133	-0.027	0.053 (160)	0.7
Complexe 3	0.140	-0.006	0.067 (140)	1.0
Complexe 4	0.089	-0.130	0.021 (219)	1.6
Complexe 5	-0.054	-0.174	-0.114 (120)	1.0
Complexe 6	-0.234	-0.371	-0.302 (137)	1.0
Complexe 7	0.063	-0.165	-0.051 (228)	1.0

[a]Measured in dimethylformamide for complexes **4**, **7** and in dichloromethane for complexes **2**, **3**, **5**, **6** with 0.1 M tetrabutylammonium perchlorate (TBAP).[b]Data from cyclic voltammetric measurements; $E_{1/2}$ is calculated as average of anodic (E_{pa}) and cathodic (E_{pc}) peak potentials $E_{1/2} = 1/2(E_{pa}+E_{pc})$; and [c]$\Delta E_p = E_{pa} - E_{pc}$ at scan rate 0.1 V/s. [d]Constant-potential coulometric data $n = i_{pa}/i_{pc}$ calculated for $1e^-$ transfer.

Table S3. Crystallographic parameter for complex **1**

Empirical formulas		$C_{38}H_{36}Cl_2N_6O_6Fe_2$ **1**	
Colour	Black	**Z**	4
Formula weight [g mol^{-1}]	855.33	**ρcalc [gcm^{-3}]**	1.427
Temperature [K]	273(2)	**F(000)**	1760
λ [Å] (Mo-Kα)	0.71073	**θ range for data Collection**	1.37- 29.99
Crystal system	monoclinic	**Index ranges**	-21<h<21, -18<k<18, -28 <l<28
Space group	*P 21/c*	**Refinement method**	Full matrix least squares on F^2
a [Å]	15.3175(7)	**Data/restraints/parameters**	11571/0/489
b [Å]	13.2070(6)	**GOF on F^2**	2.002
c [Å]	20.3269(9)	**R_1[b][I>2σ(I)]**	0.1125
α [°]	90.00	**R_1[all data]**	0.1563
β [°]	104.539(3)	**wR_2[c][I> 2σ(I)]**	0.3339
γ [°]	90.00	**wR_2 [all data]**	0.3524
Crystal size[mm]	0.28 x 0.18 x 0.14	**V [Å^3]**	3980.4(3)

Table S4. Selected bond lengths (Å) and angles (deg) of complex **1**

Complex 1			
Bond distances (Å)		**Bond angles (°)**	
Fe1-O6	1.927(5)	O6-Fe1-N6	157.3(2)
Fe1-N7	2.154(5)	O6-Fe1-N7	85.66(19)
Fe1-N6	2.128(6)	N6-Fe1-N7	74.5(2)
Fe1-Cl4	2.301(2)	O6-Fe1-O2	83.57(19)
Fe1-O4	2.268(2)	N7-Fe1-O2	81.74(19)
Fe1-O2	2.208(5)	O6-Fe1-O4	101.10(15)
		N6-Fe1-O4	96.85(16)
		N7-Fe1-O4	168.44(16)
		O2-Fe1-O4	89.66(14)
		O6-Fe1-Cl4	97.05(16)
		N6-Fe1-Cl4	93.94(16)
		N7-Fe1-Cl4	89.96(15)
		O2-Fe1-Cl4	171.61(14)
		O4-Fe1-Cl4	98.40(8)

Table S5. Computed ligand lipophilicity (log p) values by ALOGPS 2.1 and ACD/ChemSketch software program.

Compound	Calculated ligand log P (ALOGPS 2.1)	Calculated ligand log P (ACD/ChemSketch)
PhimpH	3.67	3.11±0.56
Me-PhimpH	4.00	3.28±0.58
N-PhimpH	4.72	4.34±0.56

Table S6. Geometrical parameters calculated by DFT calculations

Complex 2		**Complex 4**		**Complex 5**		**Complex 6**	
Bond distances (Å)							
Fe1-O1	1.88	Fe1-O1	1.89	Fe1-O3	1.90	Fe1-O1	1.90
Fe1-N2	2.143	Fe1-N3	2.16	Fe1-O11	1.90	Fe1-O2	1.90
Fe1-N1	2.186	Fe1-N1	2.132	Fe1-N11	2.188	Fe1-N4	2.144
Fe1-Cl1	2.317	Fe1-Cl1	2.315	Fe1-N15	2.188	Fe1-N3	2.145
Fe1-Cl2	2.313	Fe1-Cl2	2.312	Fe1-N8	2.154	Fe1-N1	2.167
				Fe1-N13	2.151	Fe1-N6	2.167
Bond angles (°)							
O1-Fe1-N2	146.3	O1-Fe1-N3	81.9	O11-Fe1-O3	100.18	O1-Fe1-O2	105.8
O1-Fe1-N1	82.9	O1-Fe1-N1	147.4	O11-Fe1-N11	84.34	O1-Fe1-N4	83.5
N2-Fe1-N1	74.04	N3-Fe1-N1	74.7	O11-Fe1-N8	89.8	O1-Fe1-N3	96.02
O1-Fe1-Cl2	97.6	O1-Fe1-Cl2	107.7	O11-Fe1-N15	98.5	O1-Fe1-N6	88.7
N2-Fe1-Cl2	93.2	N3-Fe1-Cl2	95.4	O11-Fe1-N13	157.6	O1-Fe1-N1	154.4
N1-Fe1-Cl2	154.7	N1-Fe1-Cl2	96.9	O3-Fe1-N15	84.3	O2-Fe1-N4	96.1
O1-Fe1-Cl1	108.4	O1-Fe1-Cl1	97.09	O3-Fe1-N11	98.7	O2-Fe1-N3	83.5
N2-Fe1-Cl1	97.1	N3-Fe1-Cl1	151.9	O3-Fe1-N13	89.7	O2-Fe1-N1	88.7
N1-Fe1-Cl1	92.8	N1-Fe1-Cl1	93.2	O3-Fe1-N8	157.6	O2-Fe1-N6	154.3
Cl2-Fe1-Cl1	110.8	Cl2-Fe1-Cl1	111.3	N11-Fe1-N15	175.4	N4-Fe1-N3	179.3
				N13-Fe1-N15	102.3	N3-Fe1-N6	106.18

Table S7. Calculated TD-DFT absorption signals (nm), oscillator strength (f) and nature of transitions in the complex **2**, **4**, **5** and **6**

Complex	**Wavelength (nm)**	**Osilator strength (*f*)**	**Major orbital contribution**
2	241	0.0016	HOMO-4→LUMO+2 (77%)
	323	0.0358	HOMO →LUMO+6 (43%)
	509	0.0054	HOMO-3→LUMO+1 (38%)
4	331	0.0848	HOMO-11→LUMO+3 (16%)
	383	0.0068	HOMO→LUMO+1 (29%)
	412	0.0042	HOMO-7→LUMO (49%)
	550	0.0027	HOMO-2→LUMO (38%)
	683	0.0251	HOMO→LUMO+2 (36%), HOMO→LUMO+3 (42%)
5	312	0.0002	HOMO -1→LUMO+7 (31%)
	380	0.0181	HOMO -11→LUMO+1(B) (27%)
	550	0.10	HOMO -2→LUMO+1(B) (91%)
6	310	0.145	HOMO -2→LUMO+5 (51%)
	375	0.0093	HOMO→LUMO+2 (11%), HOMO-4→LUMO (32%)
	514	0.0021	HOMO-3→LUMO+1 (85%), HOMO-1→LUMO+1 (7%)